International Journal of Materials Science and Applications
2026, Vol. 15, No. 3, pp. 113–124
https://doi.org/10.11648/j.ijmsa.20261503.14

SciencePG
Science Publishing Group

Research Article

Experimental Investigation on the Mechanical Properties of Mortar-aggregate Interface and Its Use in Meso-scale Numerical Simulation of Concrete

Yachao Zhu*

Architecture Design Department, Shenyang Aluminum and Magnesium Engineering and Research Institute Co., Ltd., Shenyang, China

Abstract

Mortar-aggregate interface is the weakest region in concrete in terms of the mechanical properties due to its relatively higher porosity compared with the surrounding bulk cement paste, which has a significant effect on the behavior of concrete when subjected to loading. As a result, the mechanical properties of the interface have been recognized as the principal condition for the meso-scale numerical modeling of the fracture process of concrete and concrete structures. In this study, the composite mortar-aggregate specimens with different surface roughness of aggregate and mortar strength were prepared to quantitatively investigate the mechanical properties of interface by means of a series of tests, including the splitting tensile test, the direct shear test and the three-point bending test. The test results indicated that the mechanical properties of interface to some extent depend on the strength grade of mortar and the roughness of aggregate surface. The failure mode largely depends on the fracture energy of mortar cohesion layer and the joint adhesion layer. It is also found that the fracture energy of interface increases with the increase of mortar strength and the roughness of aggregate surface. With purpose of providing basic constitutive model for meso-scale numerical simulation of concrete behavior, the tension softening curves of mortar-aggregate interface for different mortar strength grade were developed based on the test results. Finally, with the proposed constitutive model of interface on meso-scale, the response of plain concrete under loading were conducted using the Rigid Body Spring Model (RBSM). The numerical simulation results indicated that the expressions of tension softening curves were valid and can be successfully applied to the numerical analysis of concrete structures.

Keywords

Interface, Roughness, Bond Strength, Fracture Energy, Tension Softening Curve, Meso-scale Numerical Simulation

1. Introduction

Concrete is a composite material with a variety of inhomogeneities and structural defects of different sizes. In this contribution, on the meso level concrete is considered as a three-phase composite material consisting of mortar, aggregate, and interface between mortar and aggregate [1]. Evalution of the fracture process at meso level is useful to clarify the material characteristic of concrete [2]. Compared with cement paste, the interface between mortar and aggregate has the characteristics of the smaller density, higher porosity and lower strength. Therefore, the interface is regarded as the weakest

*Correspondence: Yachao Zhu (zhuyachao2006@163.com)

Received: 8 May 2026; **Accepted:** 17 May 2026; **Published:** 26 May 2026

region in concrete in terms of the mechanical properties [3, 4]. In the past few decades, many experimental researches have been conducted to examine the influential factors on the interface as well as the deterioration mechanism on a micro-level [5, 6]. However, the research results are difficult to associate directly with the macro-level mechanical properties of concrete; it also cannot be used in the numerical analysis of concrete [7].

Grasping the characteristics of the mortar-aggregate interface is one of the most crucial issues in predicting the mechanical behavior of concrete composites based on meso-scale simulations since the mortar-aggregate interface is the weakest region in concrete such that the properties of the mortar-aggregate interface mainly governed the mechanical behaviors of concrete [8, 9].

The bond strength of mortar-aggregate interface mainly consists of the adhesion strength, the friction strength and the interlocking strength. The former relates to the density of the cement paste around the interface, and the latter two relate to the aggregate shape and surface morphology. It has been well known that the aggregate surface should be treated roughly in order to obtain good bond properties. In the analysis of concrete behavior, the mortar-aggregate interface as a constituent of concrete can be considered as an initial defect, and the decrease of the mortar-aggregate interface thickness and volume may increase the strength of concrete [10]. The effects of aggregate surface roughness and mortar strength to bond strength of mortar-aggregate interface have not been clearly clarified and quantified. In the meso-scale numerical analysis, it is necessary to consider the mechanical properties of the interface between mortar and aggregate. The choice of constitutive relationship of interface has remarkable influence on the analysis result. However, it's not easy to measure the interfacial mechanical behaviors and few experimental analyses have been conducted.

In this paper, the composite mortar-aggregate specimens were prepared to investigate the mechanical properties of the interface by means of the splitting tensile test, the direct shear test and the three-point bending test respectively. The effects of the aggregate surface roughness and the mortar strength on the bond strength of interface were examined. Three point bending tests were conducted to determine the fracture parameters of the mortar-aggregate interface. Also, the softening curve models under tensile stress for the mortar-aggregate interface were developed based on the test results. Finally, with the proposed constitutive model of interface on meso-scale, the response of plain concrete under loading were conducted using the Rigid Body Spring Model (RBSM). The numerical simulation results indicates that the expressions of tension softening curves are valid and can be successfully applied to the numerical analysis of concrete structures.

2. Experimental Program

2.1. Materials

The composite specimens consisted of one-half mortar and one-half rock. The sizes of specimens are 150×150×150mm for splitting tensile tests and direct shear tests, 100×100×400mm for three point bending tests. All the mortars used in the composite specimens were made with ordinary Portland cement produced in Dalian, China. The 150×150×75mm and 100×100×200mm rocks were cut by a diamond saw from rough granite (also produced in Dalian, China). Medium sand was used as fine aggregate for the mortar. Two different mortars were prepared. The mix proportions of mortars are given in Table 1. The mechanical properties of mortars are shown in Table 2.

Table 1. *Mix proportions of mortars.*

Mortar type	Mix proportions Cement: Water: Sand: Water reducing agent	Material dosage (kg/m^3)			
		Cement	Water	Sand	Water reducing agent
Normal	1: 0.45: 2.5: 0	650	292.50	1625	0
High	1: 0.30: 2.0: 0.01	820	246	1640	8.20

Table 2. *Mechanical properties of mortars.*

Mortar type	W/C ratio	Compression strength (MPa)	Tensile strength (MPa)	Shear strength (MPa)	Fracture energy (N/m)
Normal	0.45	33.55	2.87	3.77	53.85
High	0.30	62.48	3.80	5.64	79.41

2.2. Specimen Preparation

The roughness of the rock surface was measured and quantified by the arithmetic mean value of roughness R_a. The roughness of the rock surface is shown in Table 3. The rocks were stored in water for 24 hours and then free water was removed before casting the mortar. Firstly, the rocks were placed in steel molds. Then, the mortars were poured into these respective molds. The specimens were then cured at 20±3 ℃ and about 95% relative humidity after casting.

Table 3. *Roughness of aggregate surfaces.*

Splitting batch	R_a (mm)	Shear batch	R_a (mm)	Bending batch	R_a (mm)
HM-1	0.618	HM-J1	0.467	HM-W1	0.602
HM-2	0.604	HM-J2	0.409	HM-W2	0.554
HM-3	0.596	HM-J3	0.671	HM-W3	0.698
HM-4	0.653	HM-J4	0.462	HM-W4	0.625
HM-5	0.550	HM-J5	0.564	HM-W5	0.727
HM-6	0.753	HM-J6	0.800	HM-W6	0.773
NM-7	0.651	NM-J7	0.680	NM-W7	0.826
NM-8	0.773	NM-J8	0.436	NM-W8	0.552
NM-9	0.747	NM-J9	0.600	NM-W9	0.855
NM-10	0.715	NM-J10	0.498	NM-W10	0.675
NM-11	0.818	NM-J11	0.827	NM-W11	0.708
NM-12	0.664	NM-J12	0.636	NM-W12	0.639

2.3. Test of Splitting Tensile

The test of splitting tensile in measuring the tensile strength of concrete and rock is used worldwide. It was proposed in 1943 by Lobo Carneiro and Barcellos firstly during the 5th Conference of the Brazilian Association for Standardization, now it is a standardized test method included in major international standards.

In this investigation, the modified splitting tensile test is used to determine the tensile strength of the mortar-aggregate interface. The splitting tensile test setup is shown in Figure 1. To prevent local failure under compression at the loading generators, two thin plywood strips (6mm width and 3mm thickness) were placed between the loading platens and the specimens to distribute the load. The loading speed was 0.05MPa/s.

2.4. Test of Direct Shear

Figure 1. *Splitting tensile test setup.*

Figure 2. *Direct shear test setup.*

The direct shear test is used widely to measure the shear strength of concrete and soil. In this study, the modified direct shear tests based on JCI-SPC3 were used to determine the shear strength of the mortar-aggregate interface. Figure 2 shows the setup of the direct shear test. The loading apparatus consists of an upper and a lower half box inside to which the specimen was mounted.

2.5. The Test of Three Point Bending

According to the fictitious crack method [11], the fracture parameters and interfacial tension softening behaviors, which can be described by stress crack width relation are the basis for meso-scale numerical analysis of concrete structures. To get the fracture parameters and tension softening behaviors of concrete materials, RILEM recommended the three point bending test for a notched beam to determine the fracture parameters.

In this study, the modified three point bending tests were used to evaluate the fracture parameters and tension softening behaviors of the mortar-aggregate interface. The setup was shown in Figure 3. All the specimens were finished the test under the displacement controlled cyclic loading mode. The loading speed was 0.1mm/min.

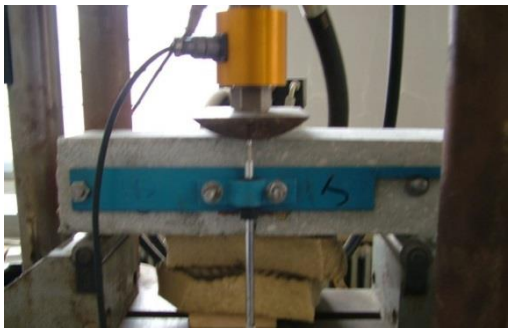

Figure 3. *Three point bending test setup.*

3. Test Results and Discussion

3.1. Bond Strength of Mortar-aggregate Interface

The splitting tensile strength can be calculated by using the following equation:

$$f_{st} = \frac{2P}{\pi A} = 0.637\frac{P}{A} \quad (1)$$

where f_{st} is the splitting tensile strength (MPa); P is the maximum load of the specimen (N); A is the area of contacting surface (mm^2).

The direct shear strength can be calculated by using the following equation:

$$f_s = \frac{P}{A} \quad (2)$$

where f_s is the direct shear strength (MPa); P is maximum load of the specimen (N); A is the area of contacting surface (mm^2).

Figure 4 and Figure 5 show the relationship between the splitting tensile strength and the direct shear strength of the mortar-aggregate interface with aggregate roughness. It can be seen that the bond strength of the mortar-aggregate interface is lower than that of the mortar. Moreover, the bond strength of the interface increases with the increase of the strength of the mortar. In addition, it can be seen that the bond strength of the mortar-aggregate interface increases as the increase of aggregate surface roughness. Especially, it has a linear relationship for the shear strength with the interface roughness, for the High mortar series through the linear regression method we can get:

$$f_s = 1.594R_a + 1.4203 \quad (3)$$

and correlation coefficient R=0.9634.

And for the Normal mortar series through the linear regression method we can get:

$$f_s = 0.5966R_a + 1.1917 \quad (4)$$

and correlation coefficient R=0.8853.

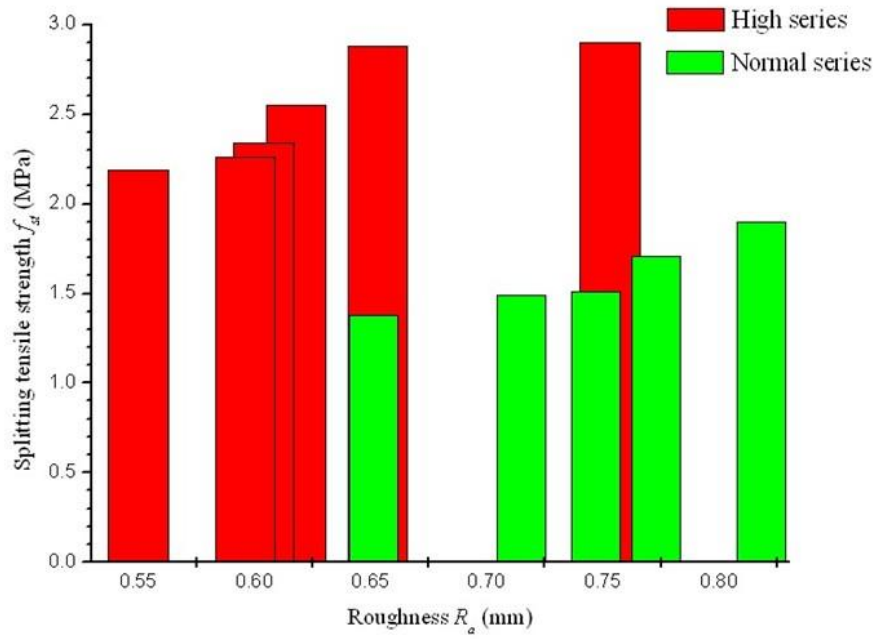

Figure 4. *Splitting strength–roughness relationship.*

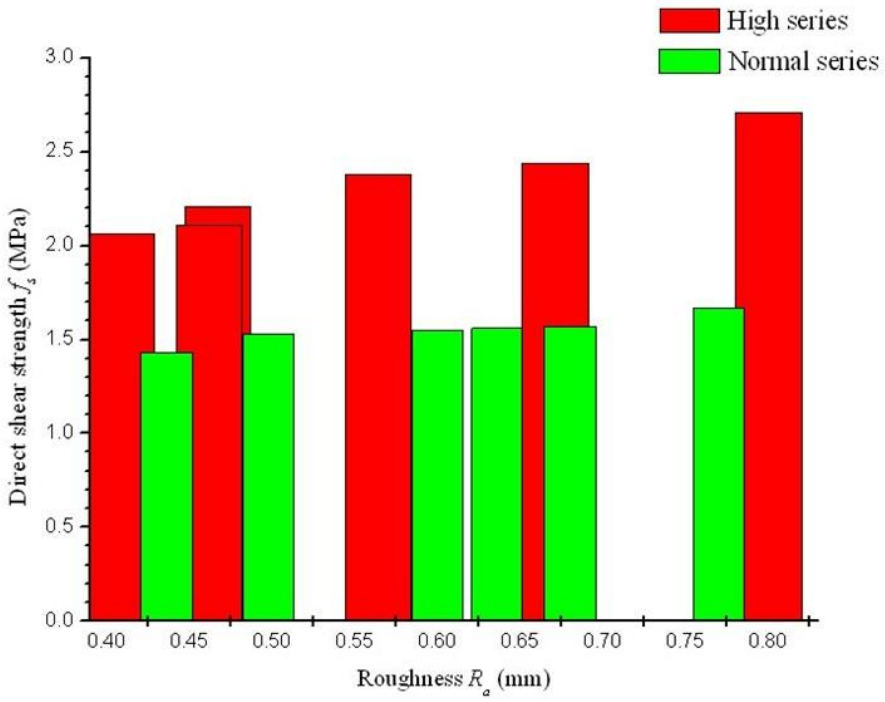

Figure 5. *Shear strength–roughness relationship.*

3.2. Failure Mode

Figure 6 shows the failure surface states of the interface after tests were presented. It can be observed that the specimens made with high strength mortar fractured at the side of the mortar near the interface, and the specimens made with normal strength mortar fractured at the joint of the interface. In comparison with the fractured mortar layer, the fractured interface of the mortar-aggregate joint line is more smooth, and the maximum load at failure is lower correspondingly. It can be seen that the volumes of mortar attached to the aggregate side are different.

Figure 6. *Typical types of fractured interface.*

Through the relationship between the bond strength with the aggregate roughness and the failure mode, it can be seen that the mortar properties play a main role in the interface bond strength. When a specimen is subjected to loading, the maximum stress of failure mainly depends on the bond efficiency between mortar and aggregate. If the bond is effective (i.e., the tensile bond strength of mortar to aggregate is greater than the strength of the interfacial mortar layer), then the failure is characterized by a fracture on the mortar side. If the bond is insufficient, a fracture will occur along the joint interface. In the high strength mortar series, the bond between mortar and aggregate is sufficient; the increase of the aggregate roughness can lead to an increase in the joint area. Accordingly, the bond strength of the adhesion layer increases more than the cohesion layer. So, it is much more sensitive to the variation of roughness R_a in comparison with the normal strength mortar series.

3.3. Fracture Parameters of Mortar-aggregate Interface

Three point bending tests on notched beams were conducted to evaluate the fracture parameters of the mortar-aggregate interface. Load-displacement curves of high strength mortar series and normal strength mortar series are shown in Figure 7.

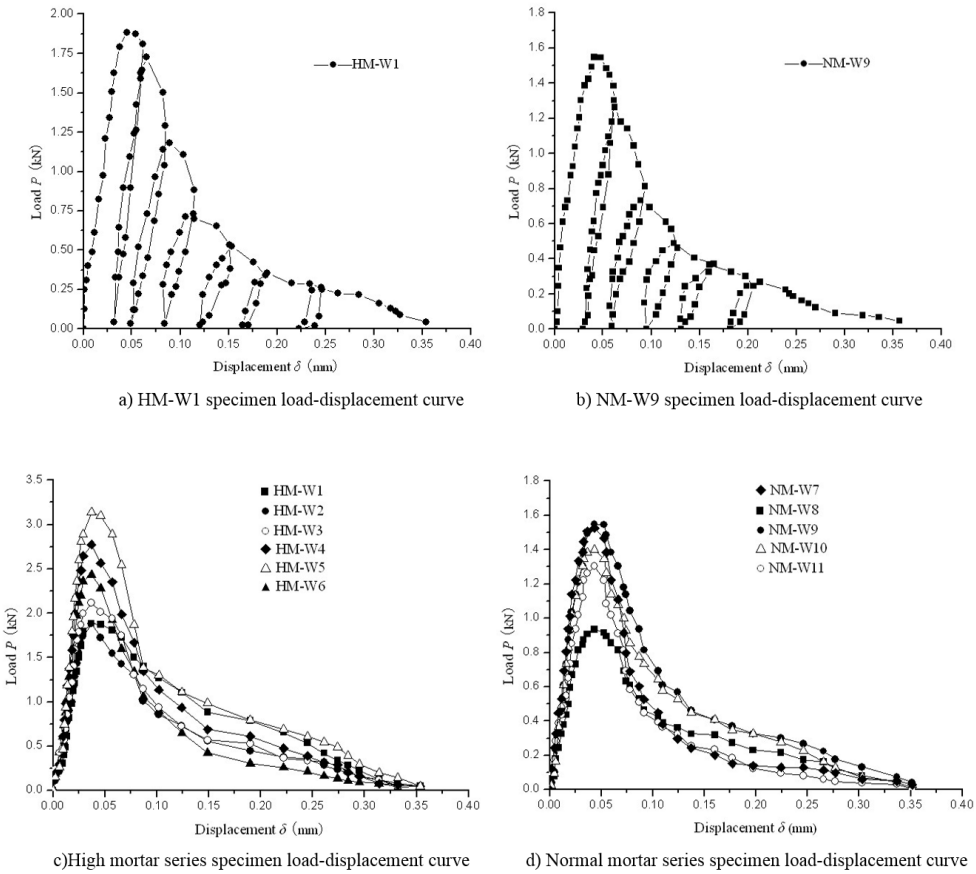

a) HM-W1 specimen load-displacement curve

b) NM-W9 specimen load-displacement curve

c)High mortar series specimen load-displacement curve

d) Normal mortar series specimen load-displacement curve

Figure 7. *Load-displacement curve.*

The interface fracture energy G_f can be obtained based on the load-displacement curves by RILEM recommended method. The fracture energy test results of interfaces are shown in Table 4.

Table 4. *Fracture energy test results of the mortar-aggregate interfaces.*

Batch	Roughness (mm)	Fracture energy G_f (N/m)
HM-W1	0.602	32.92
HM-W2	0.554	32.15
HM-W3	0.698	33.16
HM-W4	0.625	33.18
HM-W5	0.727	33.89
HM-W6	0.773	34.58
NM-W7	0.826	23.56
NM-W8	0.552	22.14
NM-W9	0.855	25.63
NM-W10	0.675	22.76
NM-W11	0.708	24.52
NM-W12	0.639	—

Based on the test results, in all cases the fracture energy of interface is smaller than the fracture energy of the mortar. With the increasing of the mortar strength, the fracture energy of the interface increases remarkably. In comparison with the mortar strength, the fracture energy is not so sensitive to the variation of roughness R_a. But it was confirmed that the aggregate roughness has effect on the fracture energy of the interface.

4. Tension Softening Curves of Mortar-aggregate Interface

Based on the modified *J*-integral method Niwa [12] proposed a new method to get the tension softening curve, which can consider the propagation of the crack width and exclude elastic displacement of the beam due to cracks. The *J*-integral is defined as the energy consumed by the crack extension and can be interpreted as all energy absorbed by the cracked specimen exclude its released elastic energy. The *J*-integral can be expressed as follows:

$$E = \int_0^{\delta} P(\delta)d\delta - \frac{1}{2}P(\delta)(\delta - \delta_P) \tag{5}$$

where $P(\delta)$ is the load of the specimen (N); δ is the displacement of the specimen (mm); δ_p is the residual displacement in a fully unloaded state (mm).

The energy E which is absorbed by the fictitious crack extension can be calculated as follows:

$$E = b\int_0^w e(\omega)\frac{a}{w}d\omega = \frac{ba}{w}\int_0^w e(\omega)d\omega \tag{6}$$

where a is the fictitious crack length (mm); b is the width of the specimen (mm); w is the crack tip opening width (mm); ω is the fictitious crack width (mm).

From equation (6), the tension softening curve can be derived. Figure 8 shows the calculated σ-w curves.

$$\begin{aligned} &\int_0^w e(\omega)d\omega = \frac{w}{ba}E(w) \\ &e(w) = \frac{1}{ba}\left[E(w) + wE'(w)\right] \\ &\sigma(w) = \frac{de(w)}{dw} = \frac{1}{ba}\left[2E'(w) + wE''(w)\right] \end{aligned} \tag{7}$$

Since the tension softening curve describes essentially the feature of the fracture process zone, various expressions of the tension softening curve such as linear, bilinear and nonlinear ones were proposed by many researchers [13]. Currently, the bilinear and Reinhardt nonlinear expressions are often used in many numerical analysis. The expression for the bilinear tension softening curve is given as follows:

$$\sigma = f_t - (f_t - \sigma_s)\frac{w}{w_s} \qquad 0 \le w \le w_s$$
$$\sigma = \sigma_s \frac{w_0 - w}{w_0 - w_s} \qquad w_s \le w \le w_0 \tag{8}$$
$$\sigma = 0 \qquad w \ge w_0$$

For this softening curve, four parameters, i.e. σ_s, w_s, f_t and w_0 are required to be determined. CEB-FIP Model Code 1990 [14] proposed to determine the parameters by the following equations:

$$\sigma_s = 0.15 f_t$$
$$w_s = 2G_F / f_t - 0.15 w_0$$
$$w_0 = \alpha_F G_F / f_t \tag{9}$$
$$G_F = G_{F0}\left(f_c / f_{c0}\right)^{0.7}$$

Reinhardt [15] proposed a nonlinear expression of the tension softening curve for concrete materials, which is written as:

$$\frac{\sigma}{f_t} = \left[1 + \left(\frac{c_1 w}{w_0}\right)^3\right] e^{\frac{-c_2 w}{w_0}} - \frac{w}{w_0}\left(1 + c_1^3\right) e^{-c_2} \tag{10}$$

where the coefficients c_1, c_2 are material constants and w_0 is the maximum crack opening width at zero stress.

For different softening curves, controlling parameters can be determined to fit the experimental results through a data fitting method. The controlling parameters are given in Table 5.

The fracture energy under each tension softening curve was calculated and also listed in Table 5. It is apparent that the fracture energies obtained by different tension softening curves were quite close to each other.

Table 5. *Determination of controlling parameters for different softening curves.*

Mortar type	f_t (MPa)	w_0 (mm)	G_F (N/m)	CEB-FIP 1990			Reinhardt		
				σs (MPa)	ws (mm)	GF (N/m)	c1	c2	GF (N/m)
Normal	1.588	0.0868	23.72	0.238	0.016	23	4.29	9.08	23.96
High	2.567	0.0931	33.31	0.385	0.0118	33	5.88	12.21	32.61

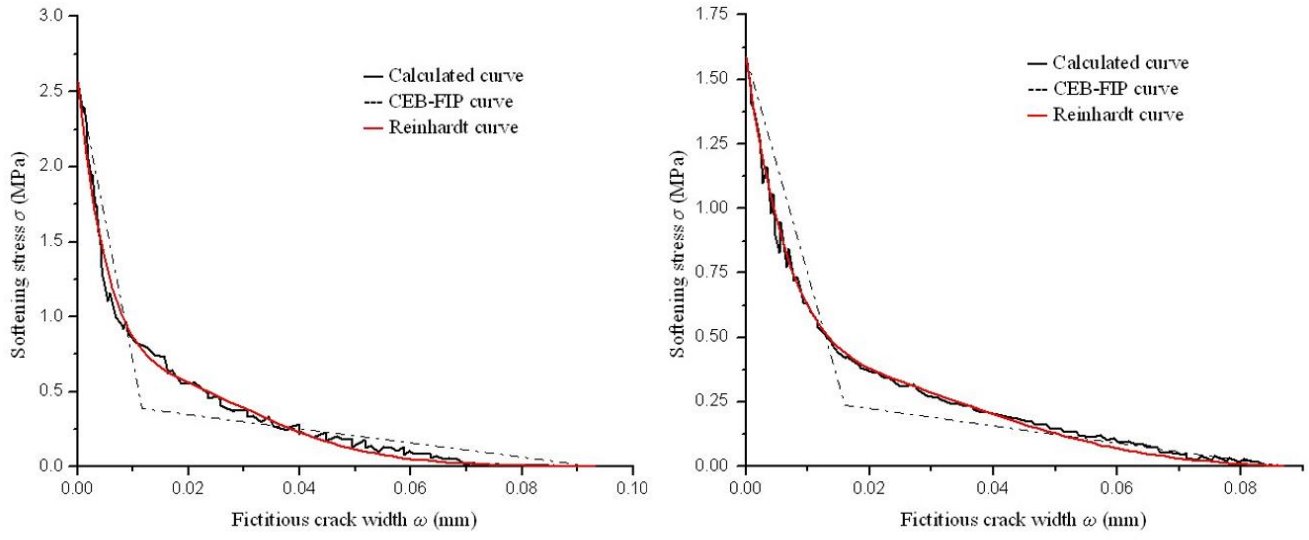

a) High mortar series b) Normal mortar series

Figure 8. *Tension softening curves.*

5. Meso-scale Numerical Simulation of Concrete

Since the meso-scale numerical analysis was introduced to simulate the failure of concrete structures, a lot of models have been developed such as the Rigid Body Spring Model [16], the Extended Distinct Element Model [17], the Beam Particle Model [18], the Particle Interface Element Mode [19]. Although numerical simulations of concrete and other quasi-brittle materials at meso-scale level have been conducted in the past few years, most of the constitutive models of the interface mechanics were empirically selected.

In this study based on the proposed tension softening curves of mortar-aggregate interface, a series of meso-scale numerical analysis of concrete samples under uniaxial compression were carried out by using the Rigid Body Spring Model (RBSM) in order to find out the effect of the different tension softening models. The specimen size is 150×150mm. The coarse aggregates are assumbed to be circular and have the volume fraction of 40% of the whole specimen (see Figure 9). The failure modes and stress-strain curves under compression loading are presented in Figure 10 and Figure 11 respectively. It can be observed that both the failure modes and stress-strain curves calculated by different tension softening curves, i.e. the curve calculated based on test data of the current study, the CEB-FIP bilinear curve and the Reinhardt's model, are very close to each other and the compressive strengths by using different softening relationships are obtained as 22.86MPa, 23.31MPa and 23.65MPa. This indicated that the expressions of different tension softening curves are valid and can be applied to the meso-scale numerical simulation of concrete structures.

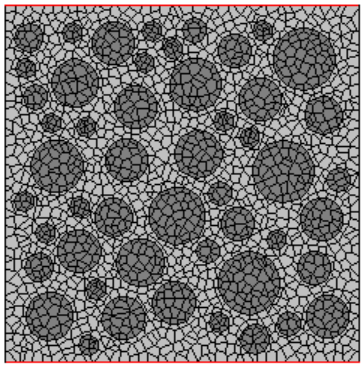

Figure 9. *Simulation model of the plain concrete specimen.*

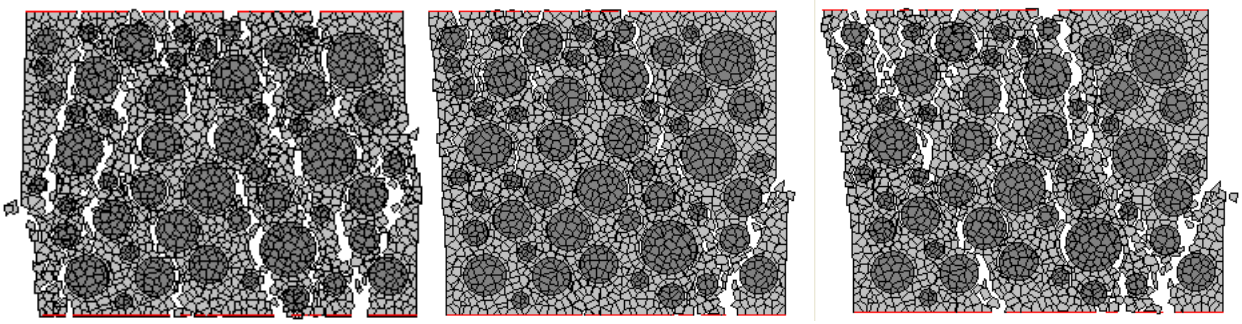

Calculated curve CEB-FIP curve Reinhardt curve

Figure 10. *Failure mode of concrete specimen.*

Experimental results about fracture mechanisams of concrete materials at the meso level indicated that crack initiate at the mortar-aggregate interface, and then propagate to the mortar part in compression tests [2, 20]. In this study based on the proposed constitutive model of interface, meso-scale numerical analysises on mortar specimens containing two aggregates were carried out using the Rigid Body Spring Model (RBSM) to reflect the crack propagation process of mortar-aggregate interface under uniaxial compression. The interface tension softening model used in this simulation was the bilinear tension softening curve proposed in this study.

The analyzed specimen is shown in Figure 12. The specimen size is 150×450mm, which is same as the experiment finished by the author Yachao Zhu. The elements number of the specimen is 2751. The properties of material in this simulation are same with the experiment. The failure mode and crack position of the specimen at axial load are shown in Figure 12, and the deformation is enlarged 10 times. Figure 13 shows the

stress strain curves of simulation and experiment. The compressive strength of the specimen calculated from the RBSM is 32.76 MPa, which is 5.67% lower than 34.73 MPa from the experiment result. As the load increased, cracks initiated at the interface of the mortar-aggregate and then propagated to the mortar side along the loading direction. The specimen failed when the cracks connected to a macro crack and ran through the specimen. This process is in good agreement with experiments in most features. It was confirmed that the simulation is capable of capturing the important features of crack the propagation process. It can well provide prediction of the damage zone in specimens.

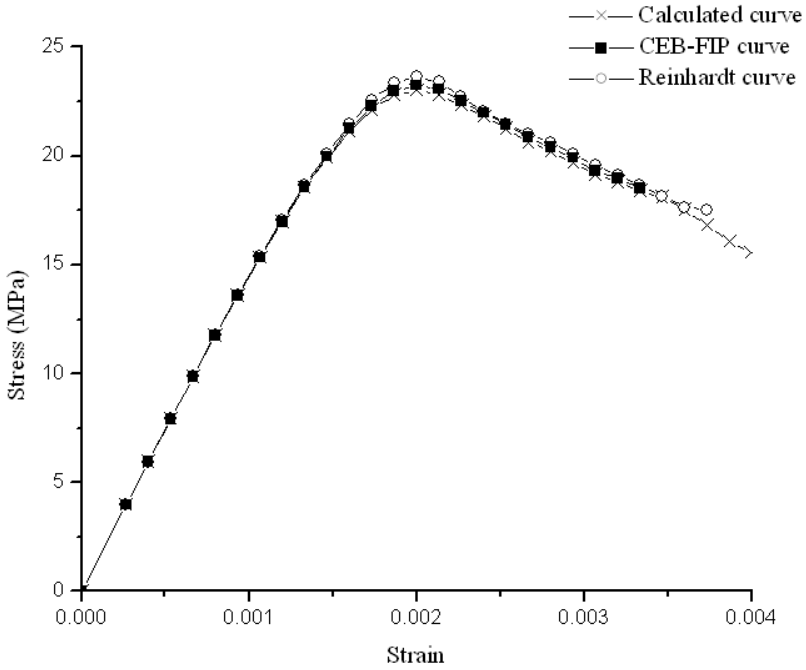

Figure 11. *Stress-strain curve of concrete specimen.*

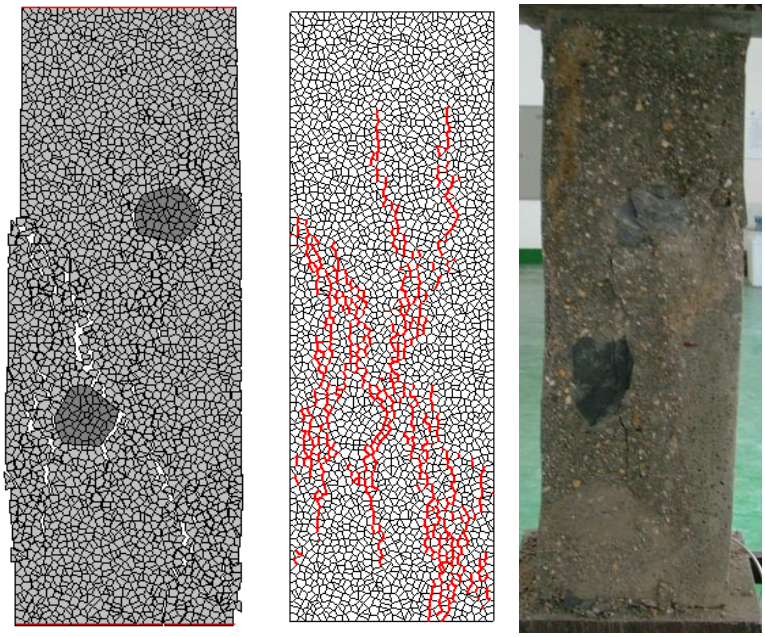

Failure mode Crack position Failure mode of experiment

Figure 12. *Failure mode and crack position of simulation and experiment.*

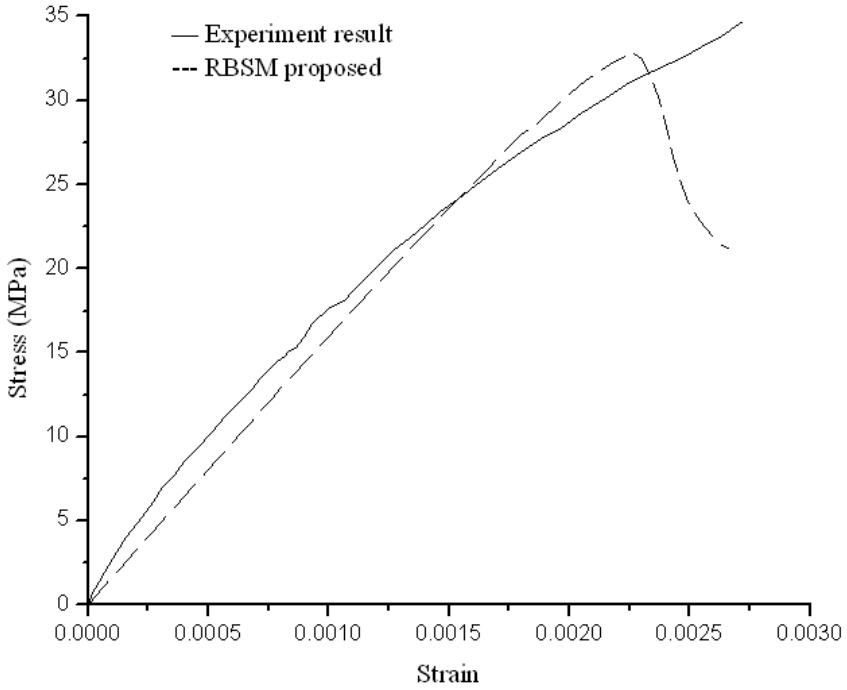

Figure 13. Stress-strain curve of simulation and experiment under uniaxial compression.

6. Conclusions

The mechanical properties of the mortar-aggregate interface, i.e., the bond strength, the fracture behavior under various loading manners and the softening curves, are systematically investigated in this study through using a set of experiments. The following conclusions can be drawn:

1. The bond strengths of mortar-aggregate interface mainly depend on the strength of mortar and the roughness of aggregate surface. It is found that the higher the mortar strength, the higher is the bond strength.

2. The fracture of failure surface largely depends on the fracture energy of mortar cohesion layer and joint adhesion layer. The fracture energy of mortar-aggregate interface depends greatly on the mortar strength and aggregate roughness.

3. Based on the modified *J*-integral, the tension-softening models for mortar-aggregate interface is established for both normal and high strength mortars by curve-fitting of the experimental data. In terms of the calculated softening curve, the mathematical expressions of bilinear and nolinear form are developed independently, which can be alternatively used in the meso-scale numerical simulation of concrete structures.

4. To check the proposed softening models and their implementation into meso-scale numerical method, the descrete element approch of Rigid Body Spring Model for plain concrete specimens is carried out. It is demonstrated that the fracture modes of concrete, as well as the crack initiation and propagation process are in good agreement with the experimental observations.

5. Most of these results are already known in a qualitative way for mortar-aggregate interface, the value of this study is to provide a quantitative fracture and mechanical properties for concrete meso-scale numerical simulation.

Abbreviations

NM	Normal Motor Type
HM	High Motor Type
Ra	The Arithmetic Mean Value of Roughness
fst	The Splitting Tensile Strength
fs	The Direct Shear Strength

Author Contributions

Yachao Zhu: Investigation, Writing – original draft

Conflicts of Interest

The author declares no conflicts of interest.

References

[1] Zaitsev, Y. B., Wittmann, F. H. (1981), “Simulation of crack propagation and failure of concrete”, Materials and Structures, 14(5), 357-365.

[2] Nagai, K., Sato, Y., Ueda, T. (2004), “Meso-scale simulation of failure of mortar and concrete by 2D RBSM”, Journal of Advanced Concrete Technology, 2(3), 359-374.

[3] Sideny, M, Young, J. F., Darwin, D. (2005), "Concrete", Translated by Wu, K. R., Zhang, X., Yao, W., et al. Beijing, Chemical Industry Press. (in Chinese).

[4] Diamond, S. (2004), "The microstructure of cement paste and concrete-a visual primer", Cement and Concrete Composites, 26(8), 919-933.

[5] Liao, K. Y., Chang, P. K., Peng, Y. N., et al. (2004), "A study on characteristics of interfacial transition zone in concrete", Cement and Concrete Research, 34(6), 977-989.

[6] Wang, X. H., Jacobsen, S., He, J. Y. (2009), " Application of nanoindentation testing to study of the interfacial transition zone in steel fiber reinforced mortar", Cement and Concrete Research, 39(8), 701-715.

[7] Chen, H. S., Sun, W., Stroeven, P. (2004), "Interfacial transition zone between aggregate and paste in cementitious composites (II): mechanical of formation and degradation of interfacial transition zone microstructure, and its influence factors", Journal of The Chinese Ceramic Society, 32(1), 71-81.

[8] Mondal, P., Shah, S. P., Marks, L. D. (2008), "Nano-scale characterization of cementitious materials", ACI Materials Journal, 105, 174-179.

[9] Mondal, P., Shah, S. P., Marks, L. D. (2009), "Nanomechanical properties of interfacial transition zone in concrete", Proceedings of Nanotechnology in Construction 3, Springer, pp. 315-320.

[10] Kim, S. M., Abu Al-Rub, R. K. (2011), "Meso-scale computational modeling of the plastic-damage response of cementitious composites", Cement and Concrete Research, 41(3), 339-358.

[11] Hillerborg, A., Modeer, M., Petersson, P. E. (1976), "Analysis of crack formation and crack growth in concrete by means of fracture mechanics and finite elements", Cement and Concrete Research, 6(6), 773-781.

[12] Niwa, J., Sumranwanich, T., Tantermisirikul, S. (1998), "New method to determine tension softening curve of concrete", Fracture Mechanics of Concrete Structures. Proceedings of FRAMCOS-3, Vol. 1, 347-356.

[13] Xu, S. L. (1999), "Determination of parameters in the bilinear, Reinhardt's and exponentially nonlinear softening curves and their physical meanings", Werkstoffe und Werkstoffpruefung im Bauwesen, Hamburg, Libri BOD, 410-424.

[14] CEB-Comite Euro-International du Beton-EB-FIP Model Code 1990. Bulletin D'Information No. 213/214, Lausanne.

[15] Reinhardt, H. W., Cornelissen, H. A. W., Hordijk, D. A. (1986), "Tensile tests and failure analysis of concrete", Journal of Structural Engineering, ASCE. 112, 2462-77.

[16] Kawai, T. (1977), "New element models in discrete strctural analysis", Journal of the Society of Naval Architects of Japan, 141, 187-193.

[17] Hakuno, M., Meguro, K. (1993), "Simulation of concrete-frame collapse due to dynamic loading", Journal of Engineering Mechanics, 119(9), 1709-1723.

[18] Zhang, D. H., Zhu, F. S., Xing, J. B. (2005), "Numerical simulation of fracture process of concrete under dynamic impact", Journal of Northeastern University (Natural Science), 26(8), 790-793.

[19] Zubelewicz, A., Bažant, Z. P. (1987), "Interface element modeling of fracture in aggregate composites", Journal of Engineering Mechanics, 113(11), 1619-1630.

[20] Nagai, K., Sato, Y., Ueda, T. (2005), "Meso-scale simulation of failure of mortar and concrete by 3D RBSM", Journal of Advanced Concrete Technology, 3(3), 385-402.